PCCP

RSC Publishing

PAPER

View Article Online
View Journal | View Issue

Cite this: *Phys. Chem. Chem. Phys.*, 2013, **15**, 12118

Role of the surface–subsurface interlayer interaction in enhancing oxygen hydrogenation to water in Pd_3Co alloy catalysts

Dhivya Manogaran[a] and Gyeong S. Hwang*[b]

Received 11th February 2013,
Accepted 19th April 2013

DOI: 10.1039/c3cp50618e

www.rsc.org/pccp

Based on density functional theory calculations, we present mechanisms underlying the improvement in the catalytic performance of Pd-based alloys for oxygen hydrogenation to water. As a model case, we consider the Pd/Pd_3Co system where one or two Pd overlayers are located on top of the bimetallic substrate. Our calculations clearly demonstrate that the subsurface Co atoms assist in facilitating the oxygen reduction reaction by lowering the activation barriers for O/OH hydrogenation with a slight increase in the O_2 scission barrier; however, we also find that the Co atoms lying below the subsurface have no significant contribution in altering the surface reactivity towards oxygen hydrogenation. The analysis of intra- and interlayer orbital interactions in the near-surface region elucidates the synergetic interplay between the surface electronic structure modification due to the underlying Co atoms (interlayer ligand effect) and the compressive strain caused by the Pd_3Co substrate. This result also brings to light the significant contribution of the out of plane (d_{xz} and d_{yz}) states in altering the surface reactivity towards O hydrogenation.

1. Introduction

The growth and progress in the widespread use of polymer electrolyte membrane fuel cells (PEMFCs) calls for a significant reduction in the amount of expensive and scarce platinum (Pt) used with the need for improving the sluggish kinetics of the oxygen reduction reaction (ORR) at the cathode. Palladium (Pd) is considered as a viable replacement for Pt because it is more abundant and less expensive, in addition to showing similar catalytic behavior and long term durability in acidic media.[1] In the past few years, studies have been dedicated towards employing Pd alloys as electrocatalysts for the ORR.[2–5] For example, alloying Pd with transition metals such as iron (Fe), cobalt (Co) and nickel (Ni) has been shown to improve the catalytic activity of Pd.[6–8] In particular, PdCo alloys with a Pd : Co atomic ratio of 3 : 1 (Pd_3Co) have been reported to exhibit significantly enhanced ORR activity relative to pure Pd.[9,10] However, Co atoms can be dissolved into the electrolyte under PEMFC operating conditions, thereby causing the gradual loss of catalytic activity.[11] The Co-leaching may lead to the formation of Pd-skin layers on Pd–Co alloy cores.[12,13]

Numerous theoretical studies using density functional theory (DFT) have been performed to understand how the bimetallic core affects the surface reactivity of the monometallic skin layer (or overlayer).[14–16] It is now well accepted that the electronic and chemical properties of the monolayer skin can be modified by two primary mechanisms; firstly, the strain effect caused by the bond length difference between the atoms in the skin layer and those in the alloy substrate, and secondly the ligand effect due to heterometallic bonding interactions with the underlying alloy. DFT has been used successfully to demonstrate the combined strain and ligand effects on the electronic structure modifications of bimetallic surfaces, and also in turn their catalytic activity towards various reactions. However, most previous studies have focused on Pt-based alloys,[17–19] so the understanding of Pd-based alloys remains relatively limited. Moreover, in many cases, a detailed analysis of interlayer orbital interactions in the near-surface region is missing despite their potential importance in understanding the alloying effect on the surface properties.

In this paper, we examine the Pd_3Co system where one or two Pd overlayers are located on top of the bimetallic substrate, with particular attention to the synergism and the relative contributions of the strain and ligand effects to the change in catalytic activity towards the ORR. We use DFT to first calculate the binding energies of main reaction intermediates (O and OH), which can be important descriptors of ORR activity,[1] and

[a] *Department of Chemistry and Biochemistry, University of Texas at Austin, Austin, Texas 78712, USA*

[b] *Department of Chemical Engineering, University of Texas at Austin, Austin, Texas 78712, USA. E-mail: gshwang@che.utexas.edu; Fax: +1-512-471-7060; Tel: +1-512-471-4847*

then the reaction energetics and activation barriers of the key steps constituting the ORR. Next, we look at alloying-induced modifications in the surface electronic structure, through careful analysis of intra- and interlayer orbital interactions and charge redistributions in the near-surface region. Based on the results, we also briefly discuss how the surface reactivity of Pd_3Co is correlated with the alloying-induced electronic structure modification.

2. Computational details

The calculations reported herein were performed on the basis of spin polarized density functional theory (DFT) within the generalized gradient approximation (GGA-PW91),[20] as implemented in the Vienna *Ab initio* Simulation Package (VASP).[21] The projector augmented wave (PAW) method[22] with a planewave basis set was employed to describe the interaction between core and valence electrons. An energy cutoff of 350 eV was applied for the planewave expansion of the electronic eigenfunctions. For the Brillouin zone integration we used a $(5 \times 5 \times 1)$ Monkhorst–Pack mesh of k points to determine the optimal geometries and total energies of the systems examined, and increased the k-point mesh size up to $(10 \times 10 \times 1)$ to reevaluate corresponding electronic structures. Reaction pathways and barriers were determined using the climbing-image nudged elastic band method[23] with eight intermediate images for each elementary step.

The model systems considered in the study are $Pd/Pd_3Co(111)$ (hereafter referred to as Pd_1Co; one Pd overlayer on the Pd_3Co substrate), $Pd/Pd/Pd_3Co(111)$ (Pd_2Co; two Pd overlayers on the Pd_3Co substrate), Pd(111) with a compressive strain of 1.77% (s-Pd; the strain imposed is equivalent to the strain imposed by the Pd_3Co substrate on Pd(111)), and pure Pd(111) (p-Pd), as illustrated in Fig. 1. For a model surface we used a supercell slab that consists of a rectangular 2×2 surface unit cell with five atomic layers, each of which contains 4 atoms. A slab was separated from its periodic images in the vertical direction by a vacuum space corresponding to seven atomic layers. While the bottom two layers of the five-layer slab were fixed at corresponding bulk positions, the upper three layers were fully relaxed using the conjugate gradient method until residual forces on all the constituent atoms became smaller than 5×10^{-2} eV Å^{-1}. The lattice constant for bulk Pd is predicted to be 3.96 Å, which is virtually identical to previous DFT-GGA calculations and also in good agreement with the experimental value of 3.89 Å.[24]

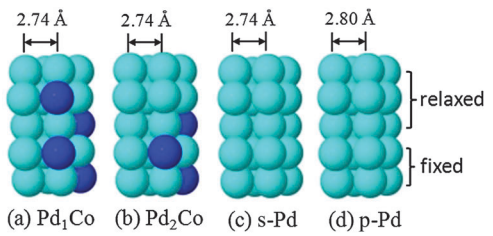

Fig. 1 Model systems used in this work. (a) $Pd/Pd_3Co(111)$ which consists of one Pd overlayer on the Pd_3Co substrate (referred to as Pd_1Co), (b) $Pd/Pd/Pd_3Co(111)$ which has two Pd overlayers on the Pd_3Co substrate (Pd_2Co), (c) Pd(111) with a compressive strain of 1.77% (s-Pd; the strain imposed is equivalent to the strain imposed by the Pd_3Co substrate on Pd(111)), and (d) pure Pd(111) (p-Pd). The cyan and blue balls represent Pd and Co atoms, respectively.

3. Results and discussion

First we calculated how the binding energies of isolated O, H, and OH (which are key intermediate species in the ORR) are affected by the alloying-induced modification of the surface electronic structure in Pd_1Co, Pd_2Co, s-Pd, and p-Pd (see Table 1). The binding energy (E_b) is given by: $E_b = E_X + E_M - E_{X/M}$, where E_X, E_M, and $E_{X/M}$ represent the total energies of the gas phase X (= O, H, OH), the slab, and the X/slab system, respectively. The O/H/OH binding energies in Pd_1Co are predicted to be lower than p-Pd by 0.21/0.06/0.13 eV. The reduction in the binding strength can be attributed to the compressive strain effect caused due to the different lattice parameters of Pd–Co and Pd–Pd. In addition, the subsurface hetero atom Co may alter the surface electronic structure; this is hereafter referred to as the 'interlayer ligand' effect to distinguish it from the 'lattice strain' effect. The O/H/OH binding energy values in Pd_2Co and s-Pd are very close to each other, implying that the presence of Co atoms in the layers below the subsurface layer may have a little effect on the surface reactivity towards O/H/OH adsorption. This result suggests that the interlayer ligand effect would be restricted to the first subsurface layer in the PdCo alloy catalysts. It is also noteworthy that O/H/OH adsorption might induce Co surface segregation,[25] but the segregation effect is beyond the scope of this work and we limit the analysis to Pd skin surface layers.

Fig. 2(a) shows the d-electron density of states (DOS) projected onto the surface Pd atoms of the Pd_1Co, Pd_2Co, s-Pd, and p-Pd systems; the Fermi level is set at zero eV. The DOS comparison between Pd_1Co and p-Pd demonstrates how the surface electronic structure is modified by the presence of Co atoms in the underlying layers and the compressive strain is induced by the $Pd_3Co(111)$ substrate. Note that the calculated lattice parameter of Pd_3Co (= 3.88 Å) is smaller than that of Pd (= 3.96 Å), imposing compression on the Pd surface layer. The compressive strain may lead to an increase in the d-orbital overlap, which in turn broadens the d-valence band while lowering its average energy.[26,27] Due to the strain effect, we can see that the Pd DOS curves of Pd_1Co become somewhat

Table 1 Calculated surface binding energies (in eV)

	O	H	OH
$Pd/Pd_3Co(111)$ [Pd_1Co]	4.52	2.73	2.41
$Pd/Pd/Pd_3Co(111)$ [Pd_2Co]	4.64	2.80	2.51
Strained Pd(111) [s-Pd]	4.64	2.76	2.50
Pure Pd(111) [p-Pd]	4.73	2.79	2.54

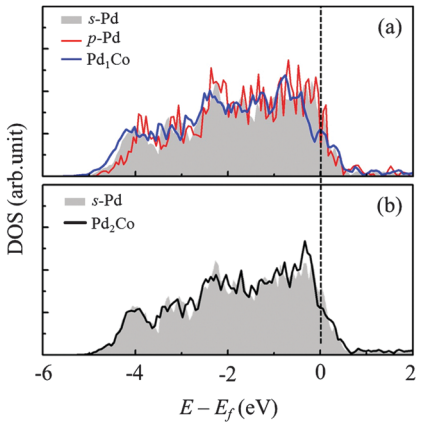

Fig. 2 (a) Density of states (DOS) projected onto the surface Pd atoms in s-Pd (shaded region), p-Pd (red solid line) and Pd_1Co (blue solid line). For comparison, the DOS plot of Pd_2Co is also shown in (b). The position of the Fermi level is indicated by the dotted line.

wider and display a slight downshift in energy; note the drastic increase in the calculated d-band center for Pd_1Co to −1.64 eV from −1.40 eV for p-Pd. In addition, there is a noticeable reduction in the DOS peak intensity near the Fermi level, and the extent of downshift in energy is more than that in s-Pd (which displays a d-band center of −1.46 eV). This suggests that the subsurface Co atoms have a significant influence on the surface electronic structure. On the other hand, the surface Pd DOS curves of s-Pd and Pd_2Co are similar, as shown in Fig. 2(b); this indicates that the interlayer ligand effect becomes insignificant when Co atoms exist below the first subsurface layer; consistently, the calculated d-band centers for Pd_2Co (−1.50 eV) and s-Pd (−1.46 eV) turn out to be comparable.

Next, we attempted to understand the surface activity of the Pd_1Co, Pd_2Co, s-Pd, and p-Pd systems towards the ORR. The ORR mechanism considered in this study consists of oxygen scission reaction followed by O/OH hydrogenation. In Table 2, we summarize the calculated total energy changes (ΔE) and activation barriers (E_a) for (A) O–O bond scission [$O_2 \rightarrow O + O$], (B) O hydrogenation [$O + H \rightarrow OH$] and (C) OH hydrogenation [$OH + H \rightarrow H_2O$]. Although the ORR is a complex process and its detailed mechanisms are still under debate, the comparisons of the reaction energetics would give important insight into the activity of different catalyst surfaces towards the ORR. Perhaps, O_2 hydrogenation [$O_2 + H \rightarrow O–OH$] and subsequent O–O bond cleavage [$O–OH \rightarrow O + OH$] would also occur. However, a previous study[28] demonstrated that their relative contributions to the H_2O formation kinetics are likely less important than the aforementioned elementary reactions on the Pd surfaces considered; according to the DFT calculations, the energy barrier for O_2 dissociation was predicted to be about 0.38 eV lower than the O_2 hydrogenation barrier on Pd(111).

Table 2 Calculated total energy changes in eV (ΔE) and activation barriers (E_a in parentheses) for (A) O_2 scission, (B) O hydrogenation, and (C) OH hydrogenation reactions. The energetically favorable adsorption sites are top-fcc-top for O_2, fcc sites for O/H, and bridge sites for OH

	(A) $O_2 \rightarrow O + O$	(B) $O + H \rightarrow OH$	(C) $OH + H \rightarrow H_2O(g)$
Pd_1Co	−1.38 (0.89)	−0.24 (0.94)	−0.37 (0.60)
Pd_2Co	−1.50 (0.88)	−0.15 (0.99)	−0.20 (0.64)
s-Pd	−1.44 (0.90)	−0.18 (0.95)	−0.25 (0.61)
p-Pd	−1.55 (0.83)	−0.10 (0.98)	−0.18 (0.74)

Our calculations predict a significantly reduced ΔE for O_2 scission on the Pd_1Co surface, compared to the p-Pd case. This can be related to the relatively weak O adsorption on Pd_1Co (see Table 1), leading to an increase of potential energy in the product side which lowers the reaction exothermicity. In addition, the activation barrier of 0.89 eV on the Pd_1Co surface is about the same as (or even slightly lower than) 0.90 eV on the s-Pd surface, while it is noticeably higher than 0.83 eV on the p-Pd surface. This may imply that the kinetics of O–O scission could be affected mainly by the compressive surface strain which causes an increase in the activation barrier.

For the O/OH hydrogenation reaction, our calculations predict a substantial reduction in the activation barrier on the Pd_1Co surface (E_a = 0.94/0.60 eV) compared to the p-Pd case (E_a = 0.98/0.74 eV). Although the predicted barrier on Pd_1Co is only slightly lower than that on s-Pd (E_a = 0.95/0.61 eV), the higher exothermicity on Pd_1Co (by 0.06/0.12 eV) may imply that the subsurface Co atom, along with the compressive surface strain, could play an important role in promoting the hydrogenation of O and OH in Pd_1Co. The notable enhancement in O/OH hydrogenation is, as expected, related to the change in relative binding strengths of reaction intermediates (O/OH/H) when alloying Pd with Co. As summarized in Table 1, the OH binding strength on Pd_1Co is reduced by 0.13 eV compared to that on p-Pd, which is less than 0.21 eV for the reduction of O binding energy [4.73 eV (p-Pd) → 4.52 eV (Pd_1Co)]; a reduction is also observed in the H binding energy, *i.e.*, E_b(H) = 2.79 eV (p-Pd) and 2.73 eV (Pd_1Co). As a result, for the O + H → OH reaction, there is an increase of potential energy in the reactant side (O + H) in comparison to the product side (OH), leading to enhanced exothermicity in O hydrogenation. Similarly, for the OH + H → $H_2O(g)$ reaction, the reduced binding strengths of OH and H on Pd_1Co may contribute to the increase of potential energy in the reactant side and consequently results in the enhanced exothermicity in OH hydrogenation.

The above results suggest that the presence of Co atoms in the subsurface layer may contribute to lowering the activation barriers of O/OH hydrogenation reactions, at the cost of a relatively small increase in the O–O scission barrier. Thus, the interlayer ligand effect also has a significant effect on the ORR activity in addition to the effect of induced compressive strain. Then, how does alloying Pd with Co lead to such surface reactivity modifications towards O_2 scission and O/OH hydrogenation? In the following section, we attempt to address this question by examining alterations in the surface–subsurface interaction induced by the presence of heteroatoms.

First, we looked at hetero-atom induced charge redistribution in the Pd_1Co, Pd_2Co, and s-Pd systems using grid based Bader charge analysis.[29] As listed in Table 3, the average surface charge per atom (q_1) is predicted to be −0.067 in Pd_1Co, which is substantially greater than −0.027 in s-Pd. This is mainly

Table 3 Calculated charge per atom in the surface (q_1) and subsurface (q_2) layers and the vertical surface–subsurface (d_1) and subsurface–2nd subsurface (d_2) distances in Å

	Pd_1Co	Pd_2Co	s-Pd
q_1	−0.067	−0.030	−0.027
q_2	+0.060	−0.010	+0.025
d_1	2.29	2.38	2.34
d_2	2.22	2.28	2.31

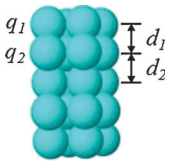

attributed to the donation of electrons from subsurface Co, leading to a substantial charge depletion in the subsurface layer (q_2 = +0.06 per atom); the Co charge state in the subsurface layer is predicted to be +0.48. We therefore, find that the charge separation (per atom) between the surface and subsurface layers ($\Delta \sim 0.13$) is significantly greater than the s-Pd case ($\Delta \sim 0.05$). We also find that the surface–subsurface interlayer distance of 2.29 Å in Pd_1Co is smaller than 2.34 Å in s-Pd, implying a Co-induced enhancement in the surface–subsurface binding. In contrast to the Pd_1Co case, both the surface and subsurface in Pd_2Co are found to have excess electrons (with charge states of −0.03 per atom and −0.01 per atom), and the surface–subsurface distance (d_1) is relatively enlarged (2.38 Å), indicating a comparatively weak surface–subsurface binding. This computational analysis predicts an average charge of +0.04 per atom in the second subsurface layer of Pd_2Co (with a charge state of +0.46 for Co) and the interlayer distance between the subsurface and second subsurface layers (d_2) is found to be 2.28 Å, which is lower than 2.31 Å in s-Pd. Therefore, we can expect an enhanced subsurface–2nd subsurface binding in Pd_2Co. Our study suggests that in addition to the surface charge distribution, the near-surface charge distribution would also influence the surface stabilization, as also demonstrated by Ramirez-Caballero *et al.*[30]

To better understand the nature of surface–subsurface interactions, we analyzed the electronic structure of the Pd_1Co, Pd_2Co, and s-Pd systems. Fig. 3 shows the DOS projected onto the d orbitals of surface Pd atoms in the systems considered. The in-plane $d_{xy+x^2-y^2}$ (= d_{xy} + $d_{x^2-y^2}$) DOS (shaded region) shows no distinct difference among the systems, indicating their relatively insignificant contribution to the changes in the surface reactivity. Looking at the out-of-plane d_z^2 and d_{xz+yz} (= d_{xz} + d_{yz}) DOS, Pd_1Co exhibits a significant downshift in energy with reduced peak intensity near the Fermi level, compared to the Pd_2Co and s-Pd cases (which display similarity). This suggests that the change of the out-of-plane d states could be a major contributor to the altered surface reactivity.

Then, how does the modification of the surface electronic structure affect the reactivity? For O adsorption, for instance, it is well known that metal d_{xz+yz} orbitals are majorly involved;[31] hence, the O binding strength is mainly determined by the extent of coupling between the O 2p and metal d states.[32] This could help explain why the O binding energy is noticeably reduced in Pd_1Co, compared to the cases of Pd_2Co and s-Pd (as reported in Table 1); that is, the reduction can be attributed

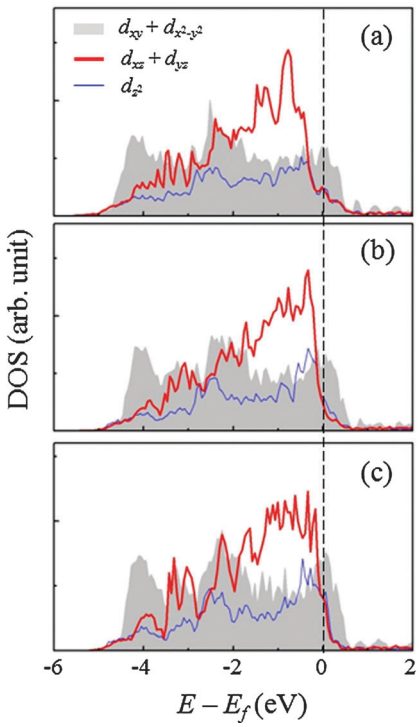

Fig. 3 Density of states (DOS) projected onto the d orbitals of the surface Pd atoms in (a) Pd_1Co, (b) Pd_2Co, and (c) s-Pd. The position of the Fermi level is indicated by the dotted line.

to the stabilization of d_{xz+yz} states that may lead to weakening of the Pd 4d and O-2p coupling.

We also turned to examining how the surface d_z^2 and d_{xz+yz} states are altered by the electronic interaction with the subsurface layer. Fig. 4 shows the orbital-decomposed d-band DOS of the subsurface Pd atoms. In Pd_1Co, the $d_{xy+x^2-y^2}$ DOS near the Fermi level are relatively suppressed and shift towards lower energies, in contrast to the densely populated in-plane states in Pd_2Co and s-Pd; the enhanced in-plane d-state interactions are apparently attributed to the presence of subsurface Co atoms. We also see a distinct downshift in energy of the d_{xz+yz} DOS from the Fermi level, which is due in part to the overlap with the stabilized in-plane $d_{xy+x^2-y^2}$ states. It can also be expected that the stabilized subsurface d_{xz+yz} states contribute to stabilization of the surface d_{xz+yz} states, to a certain degree. Similarly, the subsurface d_z^2 DOS peak near the Fermi level tends to be suppressed and downshifted, but not as significantly as in the d_{xz+yz} case; this may imply that the subsurface d_z^2 states would have a relatively weak effect, compared to the d_{xz+yz} states, on the surface stabilization and thus reactivity. This electronic structure analysis clearly demonstrates that the subsurface Co induces surface stabilization *via* enhanced surface–subsurface d_{xz+yz} interaction, which has a significant effect on the surface reactivity, while Co atoms lying below the subsurface have an insignificant contribution in altering the surface reactivity. The enhanced surface–subsurface interaction is also evidenced by the reduction in the interlayer distance in Pd_1Co relative to the Pd_2Co and strained p-Pd cases, as shown earlier.

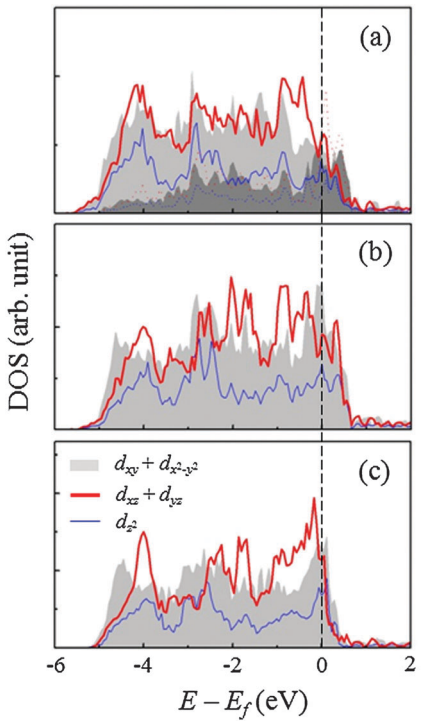

Fig. 4 Density of states (DOS) projected onto the d orbitals of subsurface Pd atoms in (a) Pd_1Co, (b) Pd_2Co, and (c) s-Pd. In (a), the DOS for subsurface Co atoms are also shown (darker grey shaded and dotted red and blue lines). The position of the Fermi level is indicated by black dotted line.

4. Summary

DFT calculations were performed to investigate the alloying-induced modifications in the surface electronic structure of Pd–Co alloys and its influence on the activity towards the oxygen reduction reaction. We considered $Pd/Pd_3Co(111)$ (referred to as Pd_1Co throughout this paper), $Pd/Pd/Pd_3Co(111)$ (Pd_2Co), Pd(111) with a compressive strain of 1.77% (s-Pd), and pure Pd(111) (p-Pd) as model systems. Due to the modification of the surface electronic structure, the binding energies of O and OH on the Pd_1Co surface are predicted to be lower by 0.21 eV and 0.13 eV, respectively, than those on the p-Pd surface. Moreover, we find that the presence of subsurface Co atoms causes a substantial reduction in the activation barriers of O/OH hydrogenation reactions (E_a for Pd_1Co = 0.94/0.60 eV; E_a for p-Pd = 0.98/0.74 eV), while the O–O scission barrier only slightly increases (E_a = 0.89 eV; E_a = 0.83 eV). This can be attributed to the synergetic interplay between the imposed compressive strain due to the Pd_3Co substrate and the interlayer ligand effect of Co atoms, as demonstrated by a thorough analysis of intra- and interlayer orbital interactions. In addition, similar O/OH binding energies for Pd_2Co and s-Pd may suggest the insignificant contribution of the interlayer ligand effect towards surface reactivity modifications, when Co atoms are present below the first subsurface. Through our electronic structure analysis, we also bring to light the possibility of an enhanced interaction between the surface and subsurface out of plane d_{xz} and d_{yz} states in Pd_1Co that has a major contribution in altering the surface reactivity. Finally, our calculations of Co induced surface and near surface charge redistribution predict an enhanced surface–subsurface charge separation and hence an enhanced surface–subsurface binding in Pd_1Co; the enhanced surface–subsurface interaction is evidenced by the reduction in the interlayer distance in Pd_1Co relative to the Pd_2Co, s-Pd and p-Pd cases. The improved understanding of the alloy substrate-induced modification of surface reactivity of metal overlayers may be helpful in designing better alloy catalysts for the oxygen reduction reaction in fuel cells.

Acknowledgements

This work was supported by the R. A. Welch Foundation (F-1535). We thank the Texas Advanced Computing Center for use of their computing resources. Helpful discussions with Hyung-Chul Ham and J. Adam Stephens are also greatly acknowledged.

References

1 J. K. Nørskov, J. Rossmeisl, A. Logadottir, L. Lindqvist, J. R. Kitchin, T. Bligaard and H. Jonsson, *J. Phys. Chem. B*, 2004, **108**, 17886.
2 Y. C. Wei, C. W. Liu, H. W. Lee, S. R. Chung, S. L. Lee, T. S. Chan, J. C. Lee and K. W. Wang, *Int. J. Hydrogen Energy*, 2011, **36**, 3789.
3 M. R. Tarasevich, V. M. Andoralov, V. A. Bogdanovskaya, D. V. Novikov and N. A. Kapustina, *Russ. J. Electrochem.*, 2010, **46**, 272.
4 H. C. Ham, G. S. Hwang, J. Han, S. W. Nam and T. H. Lim, *J. Phys. Chem. C*, 2010, **114**, 14922.
5 W. Wang, D. Zheng, C. Du, Z. Zou, X. Zhang, B. Xia and H. Yang, *J. Power Sources*, 2007, **167**, 243.
6 M. H. Shao, K. Sasaki and R. R. Adzic, *J. Am. Chem. Soc.*, 2006, **128**, 3526.
7 Y. Suo, L. Zhuang and J. Lu, *Angew. Chem., Int. Ed.*, 2007, **46**, 2862.
8 D. N. Son and K. Takahashi, *J. Phys. Chem. C*, 2012, **116**, 6200.
9 D. Wang, H. L. Xin, H. Wang, Y. Yu, E. Rus, D. A. Muller, F. J. DiSalvo and H. D. Abruna, *Chem. Mater.*, 2012, **24**, 2274.
10 O. Savadogo, K. Lee, K. Oshi, S. Mitsushima, N. Kamiya and K. I. Ota, *Electrochem. Commun.*, 2004, **6**, 105.
11 H. L. Xin, J. A. Mundi, Z. Liu, R. Cabezas, R. Hovden, L. F. Kourkoutis, J. Zhang, N. P. Subramanian, R. Makharia, F. T. Wagner and D. A. Muller, *Nano Lett.*, 2012, **12**, 490.
12 B. Li, J. Greeley and J. Prakash, *ECS Trans.*, 2009, **19**, 109.
13 D. S. Kim, T. J. Kim, J. H. Kim, E. F. Abo Zeid and Y. T. Kim, *J. Electrochem. Sci. Technol.*, 2010, **1**, 31.
14 K. Sasaki, J. X. Wang, M. Balasubramanian, J. McBreen, F. Uribe and R. R. Adzic, *Electrochim. Acta*, 2004, **49**, 3873.
15 J. R. Kitchin, J. K. Norskov, M. A. Barteau and J. G. Chen, *J. Chem. Phys.*, 2004, **120**, 10240.
16 J. R. Kitchin, J. K. Norskov, M. A. Barteau and J. G. Chen, *Phys. Rev. Lett.*, 2004, **93**, 156801.
17 V. Stamenkovic, T. J. Schmidt, P. N. Ross and N. M. Markovic, *J. Electroanal. Chem.*, 2003, **191**, 554.
18 T. Toda, H. Igarashi, H. Uchida and M. Watanabe, *J. Electrochem. Soc.*, 1999, **146**, 3750.

19 J. Greeley, I. E. L. Stephens, A. S. Bondarenko, T. P. Johansson, H. A. Hansen, T. F. Jaramillo, J. Rossmeisl, I. Chorkendorff and J. K. Norskov, *Nat. Chem.*, 2009, **1**, 552.
20 J. P. Perdew, K. Burke and M. Ernzerhof, *Phys. Rev. Lett.*, 1996, **77**, 3865.
21 G. Kresse and J. Furthmuller, *VASP the guide*, Vienna University of Technology, Vienna, Austria, 2001.
22 P. E. Blochl, *Phys. Rev. B: Condens. Matter Mater. Phys.*, 1994, **50**, 17953.
23 G. Henkelman, B. P. Uberuaga and H. Jónsson, *J. Chem. Phys.*, 2000, **113**, 9901.
24 N. W. Ashcroft and N. D. Mermin, *Solid State Physics*, Holt, Rinehart and Winston, New York, 1976.
25 C. A. Menning, H. H. Hwu and J. G. Chen, *J. Phys. Chem. B*, 2006, **110**, 15471.
26 M. Mavrikakis, B. Hammer and J. K. Norskov, *Phys. Rev. Lett.*, 1998, **81**, 2819.
27 J. R. Kitchin, J. K. Norskov, M. A. Barteau and J. G. Chen, *Phys. Rev. Lett.*, 2004, **93**, 156801.
28 H. C. Ham, J. A. Stephens, G. S. Hwang, J. Han, S. W. Nam and T. H. Lim, *Catal. Today*, 2011, **165**, 138.
29 G. Henkelman, A. Arnaldsson and H. Jónsson, *Comput. Mater. Sci.*, 2006, **36**, 354.
30 G. E. R. Caballero, Y. Ma, R. C. Tovar and P. B. Balbuena, *Phys. Chem. Chem. Phys.*, 2010, **12**, 2209.
31 A. Kokaji, A. Lesar, M. Hodoscek and M. Causa, *J. Phys. Chem. B*, 1999, **103**, 7222.
32 V. Stamenkovic, B. S. Mun, K. J. J. Mayrhofer, P. N. Ross, N. M. Markovic, J. Rossmeisl, J. Greeley and J. K. Nørskov, *Angew. Chem., Int. Ed.*, 2006, **45**, 2897.